Anticancer and Antimalarial Assays of Xanthone-Fatty Acid Hybrids: Integrative *In Vitro* and *In Silico* Evaluation

Yehezkiel Steven Kurniawan[1], Harizal Harizal[1,2], Ervan Yudha[1], Kasta Gurning[1,3], Harno Dwi Pranowo[1], Eti Nurwening Sholikhah[4], and Jumina Jumina[1*]

[1]*Department of Chemistry, Faculty of Mathematics and Natural Sciences, Universitas Gadjah Mada, Sekip Utara, Yogyakarta 55281, Indonesia*

[2]*Department of Pharmacy, Faculty of Health Sciences, Universitas Esa Unggul, Jakarta 11510, Indonesia*

[3]*Department of Pharmacy, Sekolah Tinggi Ilmu Kesehatan Senior Medan, Medan 20141, Indonesia*

[4]*Department of Pharmacology and Therapeutics, Faculty of Medicine, Public Health and Nursing, Universitas Gadjah Mada, Sekip Utara, Yogyakarta 55281, Indonesia*

**** Corresponding author:***

email: jumina@ugm.ac.id

Received: May 17, 2025
Accepted: July 10, 2025

DOI: 10.22146/ijc.106816

Abstract: *Cancer and malaria are two fatal diseases found in Indonesia over the past several years. Therefore, researchers are trying their best to find new anticancer and antimalarial agents. In the present work, we evaluated five xanthone-fatty acid hybrids, i.e., xanthyl laurate (**XL**), xanthyl myristate (**XM**), xanthyl palmitate (**XP**), xanthyl stearate (**XS**), and xanthyl oleate (**XO**), as novel anticancer and antimalarial agents. The cytotoxicity assay towards NIH3T3 reveals that xanthone-fatty acid hybrids showed a selectivity index up to 282.08, demonstrating their non-toxic profile. The MTT assay found that **XO** yielded stronger breast anticancer activity than doxorubicin as the positive control. All xanthone-fatty acid hybrids exhibited moderate antimalarial activity with IC_{50} values of 24.24–87.57 μM, lower than that of chloroquine diphosphate as the positive control (4.26 μM). As the best anticancer agent for breast cancer, the mode of action of **XO** was further studied by computational studies. The molecular docking results showed the binding energy against the HER2 protein was −45.73 kJ/mol through a hydrogen bond with Lys753. This hydrogen bond remained stable until the end of the molecular dynamics simulations for 100 ns. These findings highlight the potential application of **XO** as a new drug candidate for breast cancer treatment.*

Keywords: *bioassay; cancer; hybrid; malaria; xanthone*

■ INTRODUCTION

Cancer has been known as one of the most fatal illnesses globally [1]. In 2022, more than 20.4 million cancer patients were registered with a 49% death rate [2]. The disease is currently dominated by lung, breast, cervical, and colorectal cancers [3]. Indonesia still suffers from endemic malaria, according to the World Health Organization (WHO) report. The number of active cases keeps increasing from 0.30 million (in 2021) to 0.42 million (2023) and 0.54 million (2024), based on The Indonesian Ministry of Health report [4]. The annual data revealed that the trend keeps increasing by 30–40% for one year. However, the standard drugs such as doxorubicin, cisplatin, and 5-fluorouracil for cancer, as well as chloroquine for malaria, have been reported to generate severe side effects in normal tissues and organs [5-8]. This makes it urgent to search for new anticancer and antimalarial drugs for the coming years [9-10].

Nowadays, interest in simple drug structures without any chiral center has been increasing because of no stereochemistry issue [11]. Xanthone is one of the most promising drug candidates due to its simple chemical structure and ease of modification [12]. As of 2025, xanthone derivatives have been evaluated for

anticancer [13], antimalarial [14], antibacterial [15], antifungal [16], antidiabetic [17], and antiviral [18] applications. Especially for anticancer purposes, the bioactivity of xanthone derivatives is still not satisfactory, especially their toxic profiles to normal cells [19]. On the other hand, fatty acids are non-toxic natural products produced in plants and animals [20]. In our previous work, we have evaluated the anticancer activity of methyl oleate and ethyl oleate derivatives against HeLa, T47D, and WiDr cells representing cervical, breast, and colorectal cancer cells, respectively. The methyl oleate derivative exhibited the IC_{50} values of 24.67, 12.63, and 1.56 μg/mL against HeLa, T47D, and WiDr cells, while the ethyl oleate derivative gave lower IC_{50} values of 60.77, 30.13, and 10.05 μg/mL. Both compounds are not toxic to normal cells, providing a selectivity index of 4.02–9.18, 8.10–17.94, and 24.28–145.13 against those cancer cell lines [21]. Therefore, combining the structure of xanthone and fatty acid could maintain the bioactivity with a safe profile for normal cell lines.

Chemical modification by combining the structure of xanthone and other active chemicals becomes a primary strategy to enhance the bioactivity of organic compounds [22]. In 2003, Lundberg et al. [23] synthesized paclitaxel-oleic acid hybrid compounds as a new anticancer agent against HeLa cells. Paclitaxel reacted with oleic acid through its hydroxyl group at the 2'- and 7-position. The paclitaxel-2'-oleic acid exhibited a surpassed anticancer activity compared to paclitaxel-7-oleic acid, with an IC_{50} value of 5.5 μM. The anticancer activity of paclitaxel-2'-oleic acid was much stronger than that of paclitaxel, with an IC_{50} value of 47.7 μM. In 2009, Huan et al. [24] prepared fatty acid-doxorubicin hybrids and examined their anticancer activity against MCF-7 (breast), MDA-MB-231 (breast), and HepG2 (liver) cancer cells. Against these cell lines, doxorubicin gave the IC_{50} values of 8.3, 10.2, and 14.3 μM, respectively. In contrast, the doxorubicin-oleic acid hybrid exhibited much lower IC_{50} values, i.e., 4.7, 3.1, and 6.8 μM, against these three cancer cells. However, the evaluation of fatty acid hybrids for antimalarial application has not been reported before.

Xanthone-amino acid hybrids have been synthesized by Barbosa et al. [25] in 2024. It was reported that xanthone-amino acid hybrids showed moderate to weak anticancer activity against MCF-7 and NCl-H460 (lung) cancer cells with IC_{50} ranges of 11.61–101.77 and 11.82–66.4 μM, respectively. A series of xanthone-fatty acid hybrids, i.e., xanthyl laurate (**XL**), xanthyl myristate (**XM**), xanthyl palmitate (**XP**), xanthyl stearate (**XS**), and xanthyl oleate (**XO**), have been prepared in our previous work. These synthesized chemicals showed a potential bioactivity as antibacterial agents against *Escherichia coli* and *Staphylococcus aureus*, as well as antifungal agents against *Candida albicans* [26]. However, their anticancer and antimalarial activities have not been studied before, although the xanthone structure is active for both bioactivities.

In continuation of our study, this work aims to conduct anticancer and antimalarial assays of five xanthone-fatty acid hybrids through combined experimental *in vitro* and computational *in silico* investigations. The cytotoxicity assay is performed using NIH3T3 as normal cells, while the anticancer activity was examined utilizing 3-(4,5-dimethylthiazol-2-yl)-2,5-diphenyltetrazolium bromide (MTT) reagent against A549 (lung), HeLa, T47D, and WiDr cancer cells. The antimalarial activity of the xanthone-fatty acid hybrids is carried out through heme polymerization inhibitory activity. The most potent compound, exhibiting a higher biological activity than the standard drug, is further studied using molecular docking and molecular dynamics simulations to predict its mode of action.

■ EXPERIMENTAL SECTION

Materials

The xanthone-fatty acid hybrids, i.e., **XL**, **XM**, **XP**, **XS**, and **XO**, were synthesized as previously reported [26]. Briefly, a mixture of 3-hydroxyxanthone and fatty acid derivative in the acid chloride form is refluxed for 1 h with the aid of pyridine as the homogeneous catalyst. The target compound is isolated by using a liquid-liquid extraction stage with dichloromethane as the organic solvent, and then the target compound is chromatographically purified. The chemical structure of xanthone-fatty acid hybrids is shown in Fig. 1. The materials used in the cytotoxic and anticancer evaluations

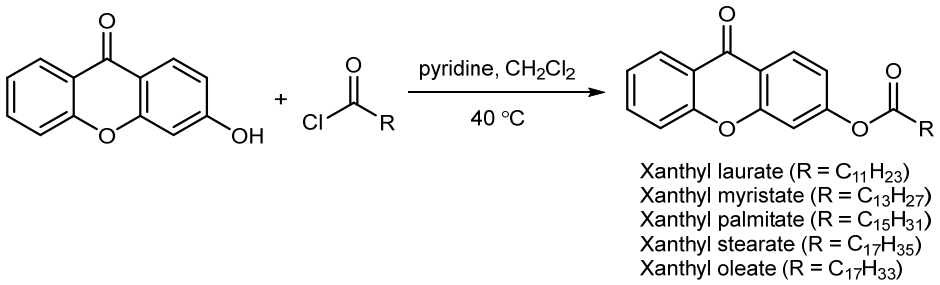

Fig 1. The chemical structure of xanthone-fatty acid hybrids

were NIH3T3, A549, HeLa, T47D, and WiDr cell lines, Dulbecco's modified eagle medium (DMEM), phosphate buffer saline (PBS), fetal bovine serum (FBS), fungizone, penicillin, streptomycin, MTT, sodium dodecyl sulfate, and dimethyl sulfoxide (DMSO). Heme, sodium hydroxide (NaOH), glacial acetic acid, and DMSO were used in the antimalarial evaluation. Doxorubicin, cisplatin, and 5-fluorouracil were used as the positive controls for the anticancer assay, while chloroquine was used as the positive control for the antimalarial assay. The chemicals used were purchased from Sigma Aldrich or Merck and had a purity of at least 95% in pro-analytical grade.

Instrumentation

The cytotoxic, anticancer, and antimalarial assay equipment was laboratory glassware, a 96-well microplate, a micropipette (Gilson and Thermo Scientific), an incubator, and an ELISA reader (BIO-RAD Benchmark). These bioassays were performed at the Laboratory of Pharmacology, Department of Pharmacology and Therapy, Faculty of Medicine, Public Health and Nursing, Universitas Gadjah Mada. The molecular docking used a computer with an Intel®CoreTMi7-13700 KF equipped with AutoDockTools-1.5.6, AutoDock4.2 [27], Gromacs 2022.5 [28], and Discovery Studio 2017 [29] software in the Austrian-Indonesian Center for Computational Chemistry, Department of Chemistry, Faculty of Mathematics and Natural Sciences, Universitas Gadjah Mada.

Procedure

Cytotoxicity and anticancer assays

The cytotoxicity assay began by incubating NIH3T3 cell lines at 310 K in a 5% CO_2 atmosphere. As much as 0.1 mL of cell culture in DMEM media was filled into the microplate to reach a density of 10^4 cells/well. Then, the dissolved test compound in DMEM media was added to the microplate at the desired concentration (1000, 500, 250, 62.50, 31.25, 15.63, and 7.81 μM) in triplicate wells. The microplate was then incubated for 1 d. Afterward, the media was carefully removed from the microplate, and 0.1 mL of 10% MTT solution was added to the microplate. The microplate was re-incubated at 310 K. After 4 h, a 0.1 mL sodium dodecyl sulfate solution was added to each well. The microplate was incubated overnight in a dark room at room temperature. The absorbance of each well was recorded using an ELISA reader at a specific wavelength of 595 nm to calculate IC_{50} and selectivity index value with the help of IBM SPSS Statistics software. The anticancer activity assay was done in a similar manner, except for replacing NIH3T3 cells with A549, HeLa, T47D, and WiDr cancer cells.

Antimalarial activity assay

The antimalarial assay began with dissolving heme in 0.2 M NaOH media to reach a final concentration of 1 mM. Meanwhile, the tested compound was dissolved in DMSO in an Eppendorf tube to reach various concentrations of 200, 100, 50, 25, 12.5, 6.25, and 3.13 μM. Both 0.10 mL of 1 mM heme solution and 0.05 mL of sample solution were added to an Eppendorf tube, followed by the addition of 0.05 mL of glacial acetic acid. The Eppendorf was incubated at 310 K for 1 d. The Eppendorf was centrifuged, and the formed hematin crystal was cleaned by using DMSO. The hematin crystal was dissolved in 0.2 mL of 0.1 M NaOH solution, and the resulting solution was placed in a 96-well microplate. This antimalarial assay was performed in triplicate. The absorbance of each well was recorded using an ELISA reader at 405 nm to calculate IC_{50} and selectivity index values.

Molecular docking

The molecular docking study was initiated by a bioinformatic approach to find the possible protein receptor targeted by the xanthone-fatty acid hybrid as an anticancer and/or antimalarial agent. The SMILES notation of the xanthone-fatty acid hybrid was submitted to the SwissTargetPrediction database to obtain possible protein receptors targeted by the xanthone-fatty acid hybrid. Then, the protein receptors involved in cancer and/or malaria diseases were collected from the Online Mendelian Inheritance in Man (OMIM) and National Center for Biotechnology Information (NCBI) databases. Both groups of protein receptors were matched to find the intersection representing possible protein receptors targeted by the xanthone-fatty acid hybrid. The selected protein receptor was then subjected to molecular docking.

The molecular docking was employed by preparing the protein and ligand structure in a .pdbqt format using AutoDockTools-1.5.6. The grid box was centered on the native ligand's binding site with a number of points of 40×40×40 with a spacing of 0.375 Å. Then, we performed the molecular docking using the AutoDock4 scoring function to estimate the binding affinity between the protein and ligand with the Lamarckian Genetic Algorithm [30] to explore the conformational space of the flexible ligand and find optimal binding poses, resulting in 100 conformations in a single run. The procedure is validated by the re-docking process, in which the root mean square deviation (RMSD) of the native ligand between before and after molecular docking does not exceed 2 Å [31]. The molecular docking of the xanthone-fatty acid hybrid was performed based on the parameters used in the re-docking process. From the molecular docking study, binding energy and binding pose between the protein and ligand can be analyzed to predict the best protein and ligand complex conformation. The non-covalent interactions between the protein receptor and ligand were visualized using Discovery Studio 2017.

Molecular dynamics simulations

The best conformation of the protein and ligand from the molecular docking was used as the input for molecular dynamics simulations in a single run to check the stability between the protein receptor and its ligand. First, the topology of the protein was prepared using the CHARMM36 force field [32], while the topology of the ligand was generated from the CGenFF server [33-34]. The complex of the protein and ligand was then solvated using the TIP3P water model [35] by extending the buffer zone of 1.2 nm in a cubic box from the center of mass of the complex. The solvated complex is neutralized by replacing the water molecules with Na^+ or Cl^- ions as the counter ions so that the particle mesh Ewald method [36] can be used for treating the electrostatic interactions, while a plain cut-off scheme was used for estimating the van der Waals interactions. The prepared system is minimized using the steepest descent algorithm, and the minimization is stopped when the steps reach 10^5 steps or the maximum force of 10^3 kJ/mol is reached. The minimized system was then equilibrated through NVT and NPT ensembles to obtain the desired conditions. The protein and ligand are restrained during the equilibration stages with a force constant of 10^3 kJ/mol/nm^2. The NVT equilibration is conducted for 500 ps and obtains a 310 K temperature using the V-rescale thermostat. Subsequently, the NPT equilibration is conducted for 500 ps and succeeds in obtaining 1 bar of pressure using the Berendsen barostat. Lastly, the production lasted for 100 ns with a timestep of 2 fs using a V-rescale thermostat and Parrinello-Rahman barostat [37], where the compressed coordinate is saved every 10 ps into the trajectory. Thus, the 100 ns trajectory was used to generate the protein-ligand complex's RMSD, root mean square fluctuation (RMSF), and hydrogen bonds.

■ RESULTS AND DISCUSSION

Cytotoxicity of Xanthone-Fatty Acid Hybrids

The cytotoxicity assay becomes the very first bioassay to examine whether five xanthone-fatty acid hybrids are toxic or non-toxic to the NIH3T3 normal cell lines. This assay is critical to ensure that the tested compounds are non-toxic to normal cells. The new anticancer or antimalarial drug will not be considered if it is unsafe for normal cells. The cytotoxicity results of xanthone-fatty acid hybrids, as well as the standard anticancer drugs, i.e., doxorubicin, cisplatin, and 5-

fluorouracil, and chloroquine as the standard antimalarial drug, are shown in Table 1. The **XL**, **XM**, **XP**, **XS**, and **XO** gave the IC_{50} values of 9754.43, 292.48, 472.34, 1076.19, and 83.38 μM, respectively. These xanthone-fatty acid hybrids are safe for NIH3T3 normal cell lines because their IC_{50} values are higher than 50 μM. The **XL** compound exhibited the highest IC_{50} value due to its shortest fatty acid chain, while the **XO** gave the lowest IC_{50} value due to its longest fatty acid chain. However, **XS** with the fatty acid chain as long as **XO** showed a higher IC_{50} value. It could be caused by the presence of a cis-double bond in **XO** that is not found in **XS**. Xanthone-fatty acid hybrids are more toxic than hydroxyxanthones and epoxidized oleate esters, as shown in Table 1. However, all xanthone-fatty acid hybrids show comparable IC_{50} values to the standard drugs, i.e., cisplatin, 5-fluorouracil, and chloroquine, but these hybrid compounds exhibit higher IC_{50} values than doxorubicin. This result is supported by the microscopic observation of NIH3T3 cell lines before and after the addition of xanthone-fatty acid hybrid or standard drugs, as shown in Fig. 2. The cellular morphologies of NIH3T3 cells are not significantly different between before and after the addition of the tested compound. In contrast, the morphology of NIH3T3 cells changed to their shrunken form after the addition of doxorubicin. These findings highlight the promising application of xanthone-fatty acid hybrids as novel bioactive agents.

Anticancer Activity of Xanthone-Fatty Acid Hybrids

After making sure that the xanthone-fatty acid hybrids are safe for normal cells, the anticancer activity of five xanthone-fatty acid hybrids has been further evaluated through MTT assay against A549, HeLa, T47D, and WiDr cancer cells. The anticancer activity results of xanthone-fatty acid hybrids and the standard anticancer drugs, i.e., doxorubicin, cisplatin, and 5-fluorouracil, are

Table 1. The cytotoxicity, anticancer, and antimalarial activities of the xanthone and oleate compounds

Compounds	IC_{50} value (μM)					
	Normal cell	A549	HeLa	T47D	WiDr	HPIA*
XL	9754.43	1743.66	135.59	34.58	1629.93	24.87
XM	292.48	2052.79	241.79	21.38	1968.42	33.46
XP	472.34	1091.75	1471.01	15.36	1700.46	24.24
XS	1076.19	1582.31	406.79	29.21	2541.50	87.57
XO	83.38	5784.71	544.29	8.57	1326.79	46.66
Doxorubicin	11.44	20.91	-	32.80	-	-
Cisplatin	384.91	-	68.42	-	-	-
5-Fluorouracil	162.95	-	-	-	19.65	-
Chloroquine	2216.92	-	-	-	-	4.26
Xanthone [13]	247.50	-	-	194.30	-	-
1-hydroxyxanthone [38-39]	7562.00	-	1198.00	248.82	1111.00	-
1,3-dihydroxyxanthone [38-40]	304.00	-	86.00	137.24	114.00	-
1,3,6-trihydroxyxanthone [38]	457.00	-	203.00	121.89	384.00	-
1,3,8-trihydroxyxanthone [38]	3395.00	-	277.00	184.00	254.00	-
1,5,6-trihydroxyxanthone [38]	224.45	-	209.00	419.00	241.00	-
1,6-dihydroxyxanthone [38]	308.32	-	322.00	450.00	322.00	-
1,6,8-trihydroxyxanthone [41]	3394.90	-	277.00	184.00	254.00	2.85
3,4-dihydroxyxanthone [42-43]	1455.80	-	-	93.20	1255.00	-
3,4,6-trihydroxyxanthone [42-43]	2510.00	-	-	43.70	38.00	-
3,6-dihydroxyxanthone [38]	1281.00	-	162.00	746.84	786.00	-
Epoxidized methyl oleate [21]	226.53		24.67	12.63	1.56	-
Epoxidized ethyl oleate [21]	244.10		60.77	30.13	10.05	-

*Heme polymerization inhibitory assay

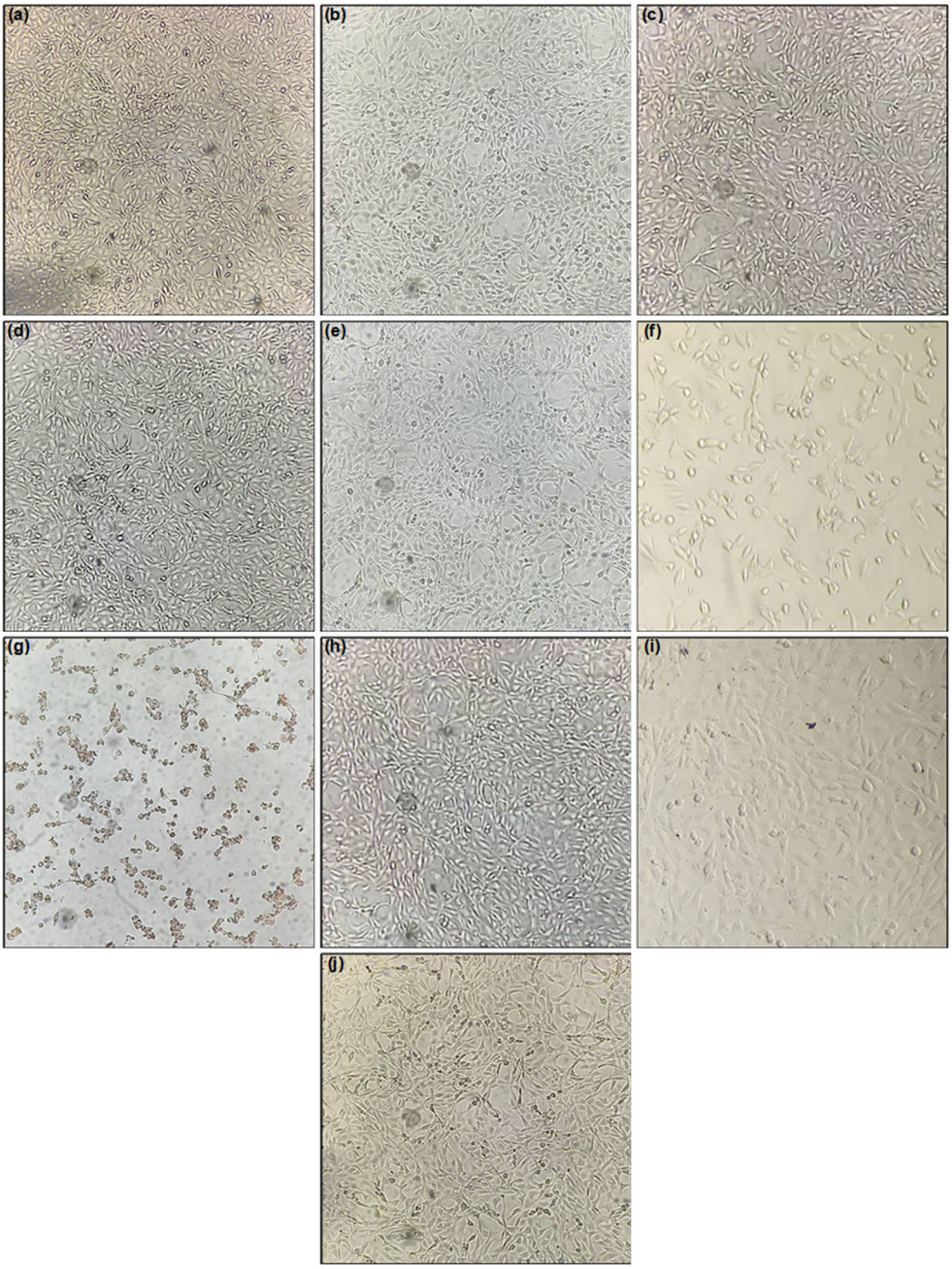

Fig 2. The morphology of NIH3T3 cells (a) before and after the addition of (b) **XL**, (c) **XM**, (d) **XP**, (e) **XS**, (f) **XO**, (g) doxorubicin, (h) cisplatin, (i) 5-fluorouracil, and (j) chloroquine at 100 μM concentration each

listed in Table 1. The **XL**, **XM**, **XP**, **XS**, and **XO** gave the IC_{50} values in a range of 34.58–1743.66, 21.38–2052.79, 15.36–1700.46, 29.21–2541.50, and 8.57–5784.71 μM, respectively. The xanthone-fatty acid hybrids show higher anticancer activity against T47D cells than HeLa, A549, and WiDr cell lines. There is no clear trend for the effect of the fatty acid chain length on the anticancer activity of xanthone-fatty acid hybrids. With the shortest fatty acid chain, **XL** gave the IC_{50} value of 1743.66 μM against A549 cells. This IC_{50} value increases for **XM** (2052.79 μM) but decreases for **XP** (1091.75 μM), and then increases again for **XS** (1582.31 μM) and further increases for **XO** (5784.71 μM). Similarly, the IC_{50} value of **XL** against HeLa cells is 135.59 μM. This IC_{50} value

increases for **XM** (241.79 μM) and **XP** (1471.01 μM) but decreases for **XS** (406.79 μM), and then increases again for **XO** (544.29 μM). On the other hand, **XL** gave the highest IC_{50} value of 34.59 μM against T47D cells. This IC_{50} value decreases for **XM** (21.38 μM) and **XP** (15.36 μM) but increases for **XS** (29.21 μM), and then decreases again for **XO** as the lowest one (8.57 μM). Meanwhile, the IC_{50} value fluctuates for **XL** (1629.93 μM), **XM** (1968.42 μM), **XP** (1700.46 μM), **XS** (2541.50 μM), and **XO** (1326.79 μM) against WiDr cells. Compared with hydroxyxanthones and epoxidized oleate esters (Table 1), xanthone-fatty acid hybrids showed stronger anticancer activity against HeLa and T47D cancer cells but weaker activity against WiDr cancer cells.

According to Tanamatayarat et al. [44], the anticancer activity is categorized as very active (IC_{50} < 5 μM), active (IC_{50} = 5–10 μM), moderate (IC_{50} = 10–50 μM), and inactive (IC_{50} > 50 μM). Therefore, only **XO** is found to be an active anticancer agent against T47D cancer cells. Meanwhile, the other xanthone-fatty acid hybrids show moderate anticancer activity against T47D cancer cells. The microscopic observation of T47D cell lines before and after the addition of xanthone-fatty acid hybrid or doxorubicin as the standard drug is shown in Fig. 3. The cellular morphologies of T47D cells are significantly different before and after the addition of the tested compound due to their potential anticancer activity. In contrast, the morphology of A549, HeLa, and

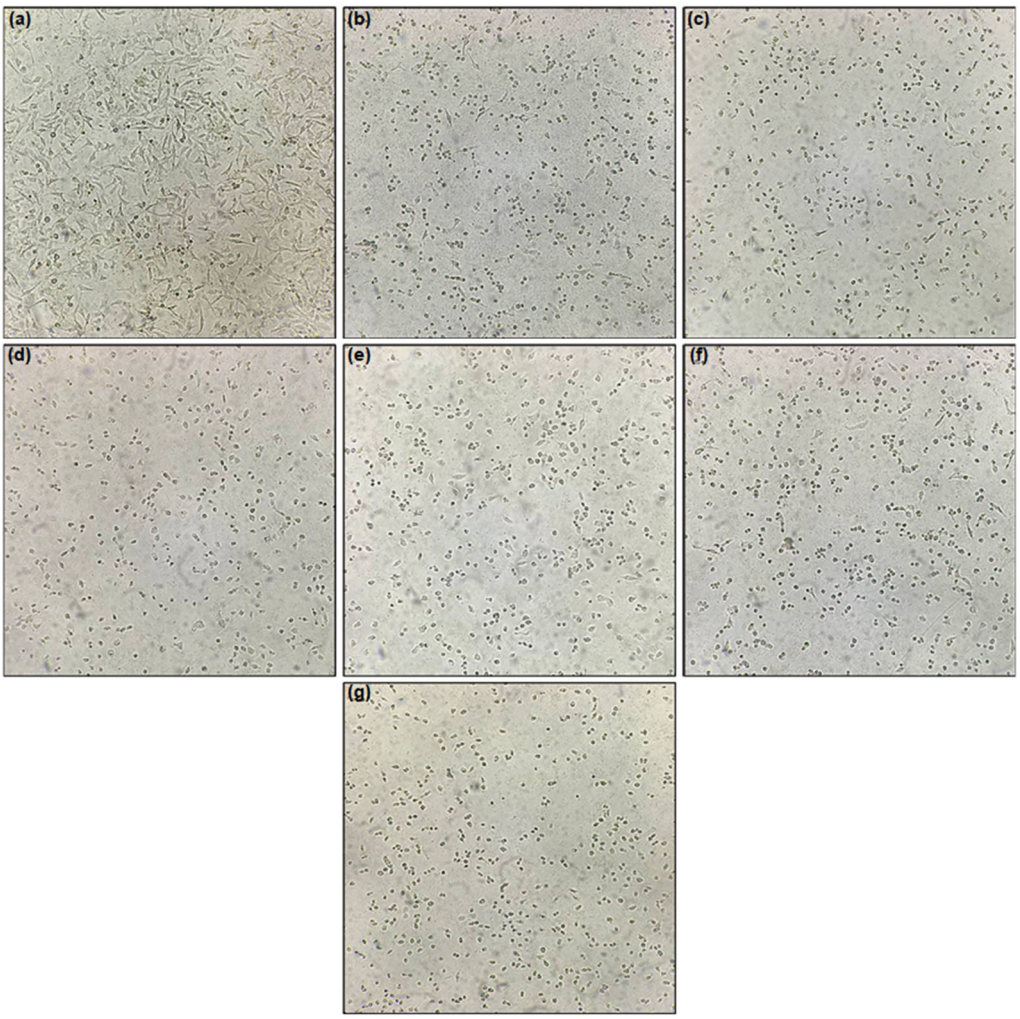

Fig 3. The morphology of T47D cells (a) before and after the addition of (b) **XL**, (c) **XM**, (d) **XP**, (e) **XS**, (f) **XO**, and (g) doxorubicin at 100 μM concentration each

WiDr cells has no notable alterations due to the lack of anticancer activity of xanthone-fatty acid hybrids. Compared to doxorubicin as the standard anticancer drug, **XO**, **XP**, **XM**, and **XS** exhibit a surpassed anticancer activity, while **XL** shows a comparable anticancer activity against T47D cells. On the other hand, all xanthone-fatty acid hybrids are inactive against A549, HeLa, and WiDr cancer cells because their IC_{50} values are higher than 50 μM. Instead of that, their IC_{50} values against A549, HeLa, and WiDr cells are higher than those of doxorubicin, cisplatin, 5-fluorouracil.

An effective anticancer drug shall be toxic to cancer cells but safe for normal cells. As a quantitative parameter for this observation, the selectivity index is defined as the ratio of the IC_{50} value against normal cells over the IC_{50} value against cancer cells. The selectivity indexes of xanthone-fatty acid hybrids and the standard anticancer drugs, i.e., doxorubicin, cisplatin, and 5-fluorouracil, are tabulated in Table 2. The **XL**, **XM**, **XP**, **XS**, and **XO** gave the selectivity index values in a range of 5.59–282.08, 0.14–13.68, 0.28–30.75, 0.42–36.84, and 0.01–9.73 μM, respectively. The xanthone-fatty acid hybrids show a higher selectivity index against T47D cells than HeLa cells. Moreover, the selectivity index of these compounds is much lower against both A549 and WiDr cells, except for the **XL**. Unfortunately, no clear trend is observed for the effect of the fatty acid chain length on the selectivity index parameter. With the shortest fatty acid chain, **XL** gave a selectivity index of 5.59 against A549 cells. This selectivity index significantly decreases for **XM** (0.14) but increases for **XP** (0.43) and **XS** (0.68), and then drastically decreases for **XO** as the lowest one (0.01). Similarly, the selectivity index of **XL** against WiDr cells is 5.98. This selectivity index significantly decreases for **XM** (0.15) but increases for **XP** (0.28) and **XS** (0.42), and then drastically decreases for **XO** (0.06). The same trend is also

Table 2. The selectivity index of the reported xanthone and oleate compounds

Compounds	Selectivity index				
	A549	HeLa	T47D	WiDr	HPIA*
XL	5.59	71.94	282.08	5.98	392.22
XM	0.14	1.21	13.68	0.15	8.74
XP	0.43	0.32	30.75	0.28	19.49
XS	0.68	2.65	36.84	0.42	12.29
XO	0.01	0.15	9.73	0.06	1.79
Doxorubicin	0.55	-	0.35	-	-
Cisplatin	-	5.63	-	-	-
5-Fluorouracil	-	-	-	8.29	-
Chloroquine	-	-	-	-	520.40
Xanthone [13]	-	-	-	1.27	-
1-Hydroxyxanthone [38-39]	-	6.31	30.39	6.81	-
1,3-Dihydroxyxanthone [38]	-	3.53	2.22	2.67	-
1,3,6-Trihydroxyxanthone [38]	-	2.25	3.75	1.19	-
1,3,8-Trihydroxyxanthone [38]	-	12.26	18.45	13.37	-
1,5,6-Trihydroxyxanthone [38]	-	1.07	0.54	0.93	-
1,6-Dihydroxyxanthone [38]	-	0.96	0.69	0.96	-
1,6,8-Trihydroxyxanthone [41]	-	12.26	18.45	13.37	1189.52
3,4-Dihydroxyxanthone [42-43]	-	-	15.62	1.16	-
3,4,6-Trihydroxyxanthone [42-43]	-	-	57.44	66.05	-
3,6-Dihydroxyxanthone [38,43]	-	7.91	1.72	1.63	-
Epoxidized methyl oleate [21]	-	9.18	17.94	145.13	-
Epoxidized ethyl oleate [21]	-	4.02	8.10	24.28	-

*Heme polymerization inhibitory assay

noticed for T47D cells. The **XL** gives the highest selectivity index of 282.08 against T47D cells. This selectivity index significantly decreases for **XM** (13.68) but increases for **XP** (30.75) and **XS** (36.84), and then decreases for **XO** (9.73). On the other hand, xanthone-fatty acid hybrids show a different trend for HeLa cells. The **XL** gave a selectivity index value of 71.94 against HeLa cells. This IC_{50} value decreases for **XM** (1.21) and **XP** (0.32) but increases for **XS** (2.65) and then decreases again for **XO** (0.15).

Widiandani et al. [45] reported that a non-toxic anticancer agent is confirmed when the selectivity index value is higher than 2. Only the **XL** meets this criterion for all cancer cells, as its selectivity index is in the range of 5.59–282.08. In accordance with the anticancer activity results, all xanthone-fatty acid hybrids show a non-toxic profile when applied as the anticancer agent against T47D cells. Even though **XL**'s selectivity index is the highest (282.08), its anticancer activity against T47D cells is the weakest (IC_{50} = 34.58 μM). In contrast, **XO** gives the lowest selectivity index, i.e., 9.73, even though it is still higher than the standard defined by Widiandani et al. [45]. **XO** exhibits the most potent anticancer activity against T47D cells (IC_{50} = 8.57 μM). This finding demonstrates that **XO** is the most promising anticancer agent for T47D cells with a non-toxic profile for normal cells.

Antimalarial Activity of Xanthone-Fatty Acid Hybrids

The antimalarial activity of five xanthone-fatty acid hybrids has also been investigated through a heme polymerization inhibitory assay mimicking the physiological condition of *Plasmodium falciparum*. The antimalarial activity results of xanthone-fatty acid hybrids and the standard antimalarial drug, i.e., chloroquine, are shown in Table 2. The **XL**, **XM**, **XP**, **XS**, and **XO** gave the IC_{50} values of 24.87, 33.46, 24.24, 87.57, and 46.66 μM, respectively. Similar to the anticancer data, the fatty acid chain length has no apparent effect on the antimalarial activity of xanthone-fatty acid hybrids. With the shortest fatty acid chain, **XL** gave the IC_{50} value of 24.87 μM. This IC_{50} value increases for **XM** (33.46 μM) but decreases for **XP** (24.24 μM), and increases again for **XS** (87.57 μM), and then decreases again for **XO** (46.66 μM). The antimalarial activity is categorized based on the classification of IC_{50} values by Batista et al. [46], i.e., very active (IC_{50} < 1 μM), active (IC_{50} = 1–20 μM), moderate (IC_{50} = 20–100 μM), and inactive (IC_{50} > 100 μM). According to this justification, all xanthone-fatty acid hybrids showed moderate antimalarial activity. However, their antimalarial activity is much weaker than that of chloroquine as the positive control. This result indicates that xanthone-fatty acid hybrids are unsuitable for new antimalarial agents because they could not replace chloroquine with such weaker antimalarial activity.

Molecular Docking and Molecular Dynamics Simulations

Molecular docking and molecular dynamics simulations were performed to predict the ability of **XO** to bind to the active site of the protein receptor, which may explain its anticancer activity. The possible targeted receptor of **XO** is revealed by submitting its SMILES notation to the SwissTargetPrediction database. The possible targets of **XO**, as demonstrated by the SwissTargetPrediction database, are listed in Table S1. Among the 103 revealed receptors, 94.2% of targets are related to breast cancer, including the HER2 receptor. The HER2 receptor has been reported to promote rapid growth and activate anti-apoptosis and proliferative signals of breast cancer cells [47]. The HER2 receptor is overexpressed by 20% in cancer cells compared to normal cells, and it was reported that HER2 inhibition caused higher T47D sensitivity to the anticancer drugs [48-50]. Therapies that primarily target the HER2 pathway have been shown to be effective, including monoclonal antibodies and tyrosine kinase inhibitors [51]. This kind of therapy could lower the occurrence of recurrence, as well as overcome cancer metastasis and resistance [52]. Therefore, HER2 was selected as the potential receptor for the *in silico* studies of **XO** as a breast cancer anticancer agent.

The HER2 receptor is retrieved from the Protein Data Bank with a PDB ID of 3PP0. The validity of

molecular docking is confirmed from the re-docking studies when the RMSD value does not exceed 2 Å [31]. The RMSD value of the re-docking of 2-{2-[4-({5-chloro-6-[3-(trifluoromethyl)phenoxy]pyridine-3-yl}amino)-5*H*-pyrrolo[3,2-d]pyrimidin-5-yl]ethoxy}ethanol as the native ligand is found to be 1.64 Å, showing the validity of the re-docking process. Using the same docking parameters, **XO** was docked on the active site of the HER2 receptor. Fig. 4(a) shows that **XO** matched well with the structure of the native ligand on the active site of the HER2 receptor. The non-covalent interactions of native ligand and **XO** on the active site of the HER2 receptor are shown in Fig. 4(b) and 4(c), respectively. The xanthone structure of **XO** formed 2 carbon-hydrogen bonds with Leu785 and Asp863, 1 pi-amide bond with Phe864, 1 pi-sigma bond with Leu796, 4 pi-alkyl bonds with Lys753, Met774, Leu785, and Leu796, and 5 van der Waals bonds with Ile767, Glu770, Ala771, Ser783, and Arg784. Besides, the oleate structure of **XO** formed a hydrogen bond with Lys753 and 15 van der Waals bonds with Leu726, Gly727, Ser728, Val734, Ala751, Thr798, Gln799, Leu800, Met801, Gly804, Cys805, Arg849, Asn850, Leu852, and Thr862. Compared with the native ligand and doxorubicin (Fig. 4(b) and 4(d)), the non-covalent interactions with Ile767 and Arg784 are only found for **XO**. Aertgeerts et al. [53] and Fitria et al. [54]

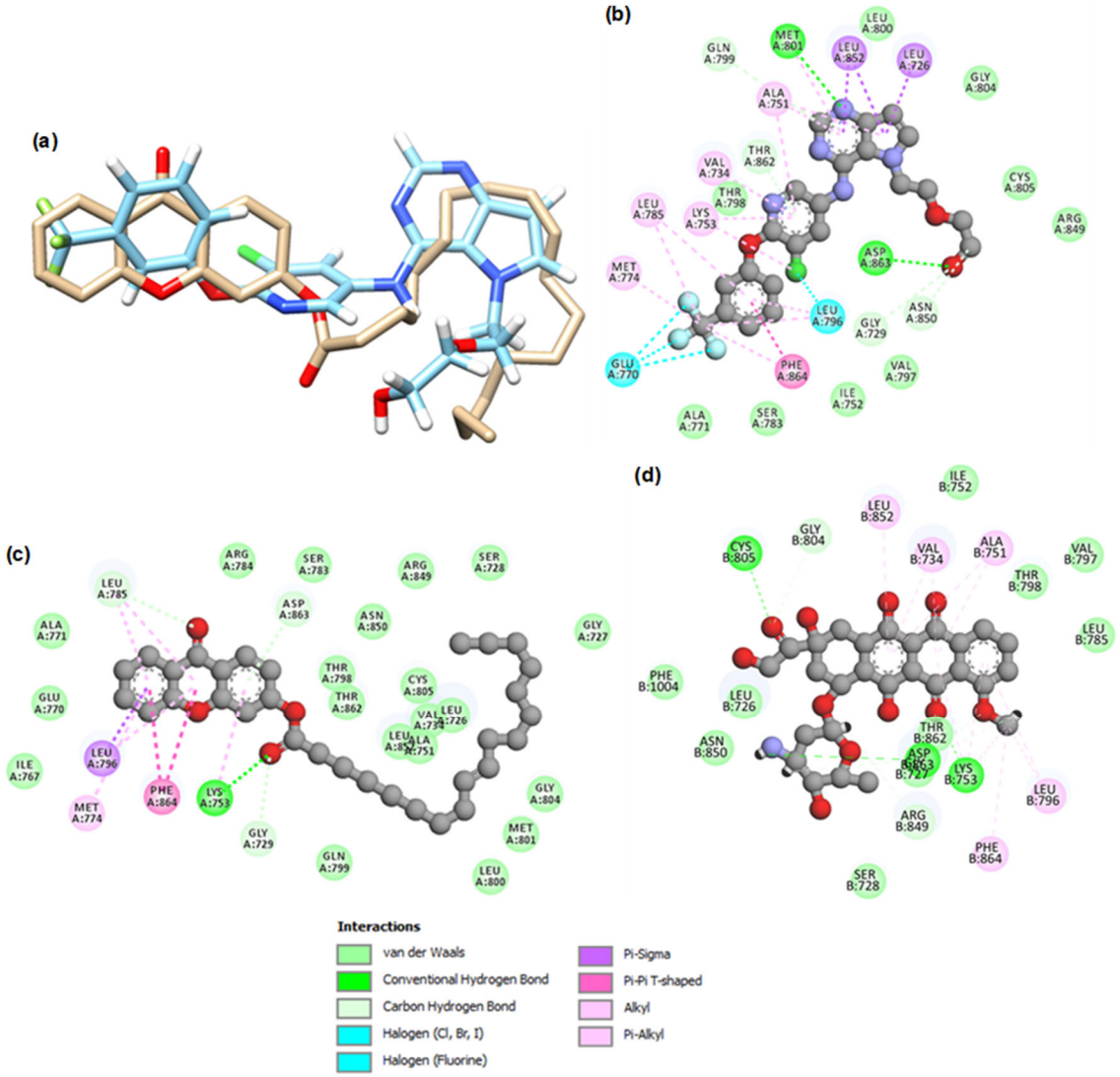

Fig 4. (a) Superimposed structure of **XO** and native ligand, and non-covalent interactions between (b) native ligand, (c) **XO**, and (d) doxorubicin on the active site of HER2 receptor

reported that amino acid residues of Leu726–Val734 and Lys753 are crucial for the ATP binding site to activate the HER2 receptor. Among the **XO**, it formed bonds with Leu726, Val734, and Lys753, indicating its ability to deactivate the physiological function of the HER2 receptor. Quantitatively, the **XO** generates a binding energy of −45.73 kJ/mol due to the formed non-covalent interactions.

To examine the binding stability of **XO** with Leu726, Val734, and Lys753 residues, we also carried out the molecular dynamics simulation for 100 ns at 310 K. The molecular dynamics simulation results, i.e., RMSD, RMSF, and the number of hydrogen bonds, are depicted in Fig. 5. RMSD describes the difference between the complex's backbone from its initial to final conformation [55] while RMSF describes how far atomic positions deviate from the starting coordinate [56-57]. During the molecular dynamics simulations, the RMSD value of the HER2-**XO** complex never touches the maximal threshold value of 3 Å (Fig. 5(a)) [58-60]. The average RMSD value is 1.77 Å, demonstrating the stability of the HER2-**XO** complex during the molecular dynamics simulations. In contrast, the average RMSD value for HER2-doxorubicin is 6.07 Å, revealing that doxorubicin is less stable than **XO** in the active site of the HER2 receptor.

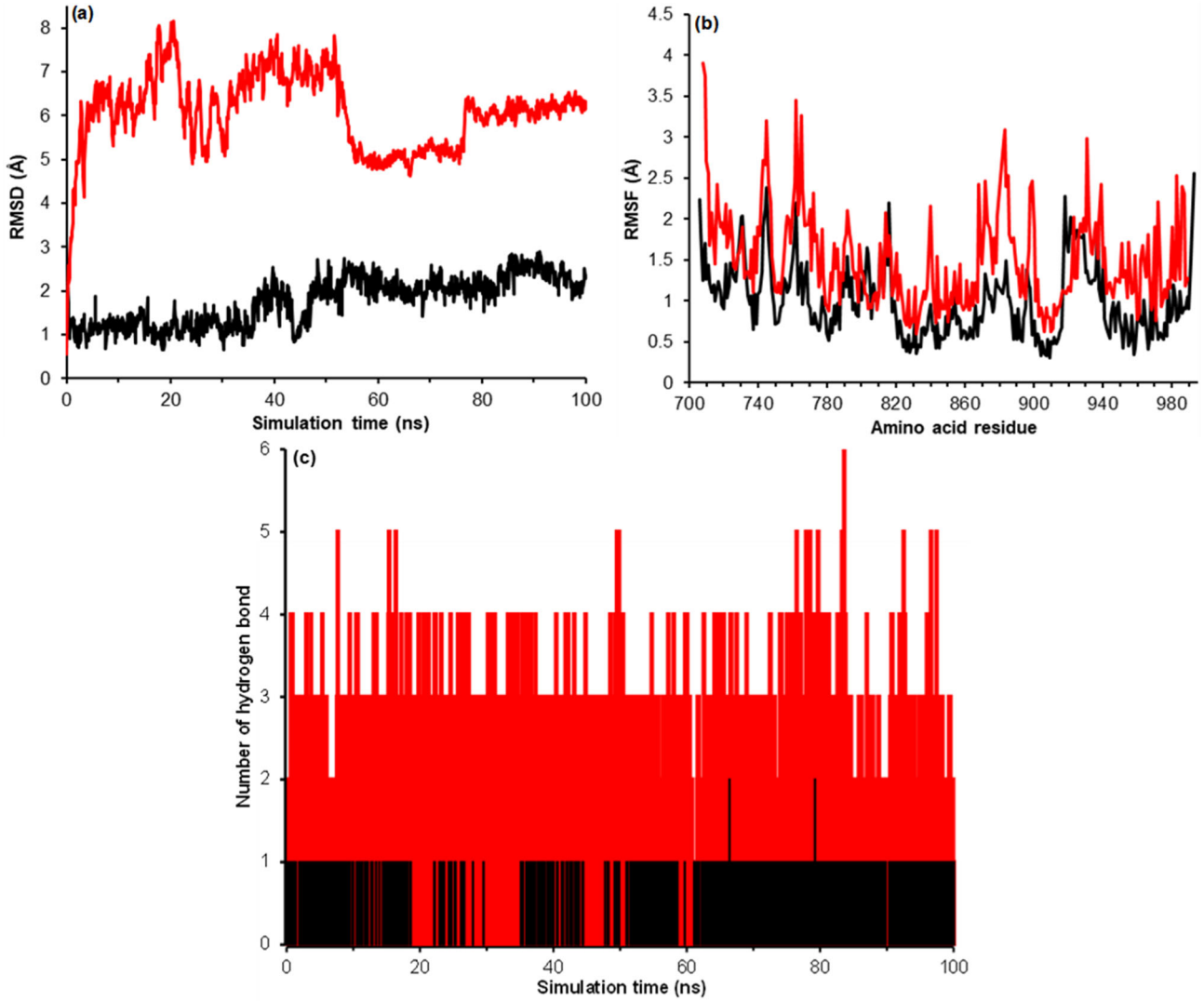

Fig 5. (a) RMSD, (b) RMSF, and (c) number of hydrogen bonds during the molecular dynamics simulations for 100 ns for **XO** (black) and doxorubicin (red)

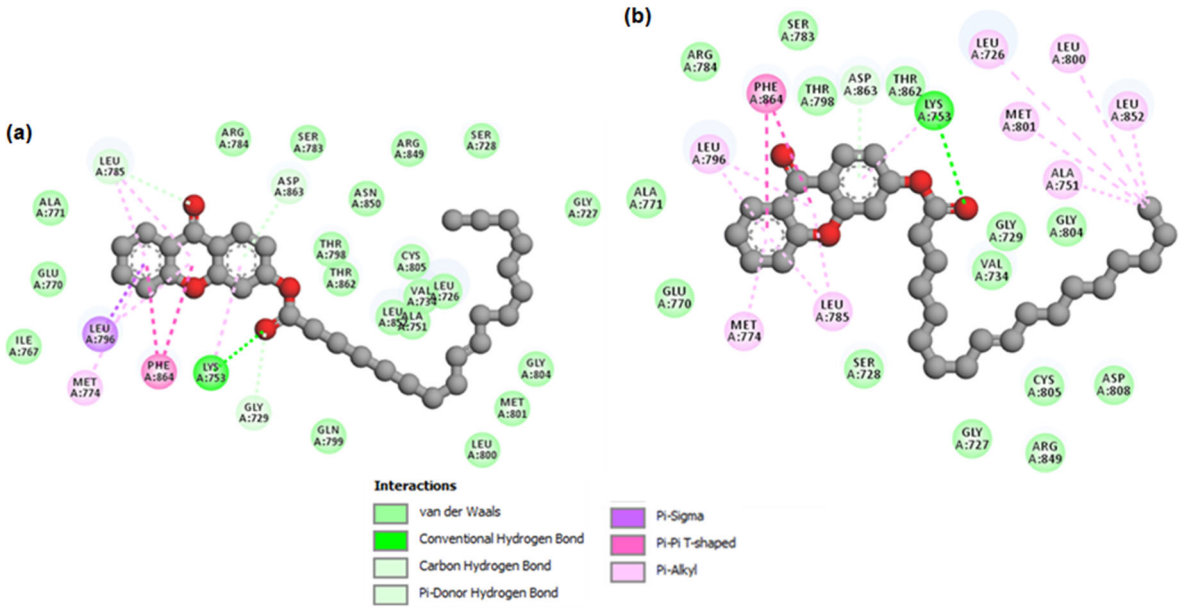

Fig 6. The non-covalent interactions between **XO** on the active site of HER2 receptor at the (a) and (b) final molecular dynamics simulations

The RMSF data reveal that only residues Ala706, Ala730, Asp745, Lys762, Arg816, Phe918, and Asp993 give RMSF values higher than 2 Å (Fig. 5(b)). Fortunately, **XO** does not interact with all of those residues, thus contributing to the stable conformation of **XO** on the active site of the HER2 receptor. The average RMSF value is 1.00 Å, demonstrating the stability of the HER2 receptor's structure during the molecular dynamics simulations. On the other hand, the average RMSF data for HER2-doxorubicin is 1.54 Å, which is higher than for the HER2-**XO** complex. As revealed in Fig. 5(c) and 6, the hydrogen bond with Lys753 and non-covalent interactions with Leu726 and Val734 are still found after the molecular dynamics simulations, confirming that there is one hydrogen bond after the molecular dynamics simulations. Even though doxorubicin could generate more hydrogen bonds in the HER2's active site, these hydrogen bonds have no sound due to their instability. These results indicate that the HER2 inhibition becomes the action mode of **XO** as a novel breast cancer anticancer agent.

■ CONCLUSION

To conclude, we have confirmed that xanthone-fatty acid hybrids showed inactive to active anticancer activity and moderate antimalarial activity with non-toxic profiles against normal cell lines. The anticancer activity of xanthone-fatty acid hybrids against T47D cells is stronger than that against HeLa cells and much stronger than against A549 and WiDr cells. However, there is no clear trend for the effect of the fatty acid chain length on the anticancer and antimalarial activities of xanthone-fatty acid hybrids. As the most potent compound, **XO** gave the lowest IC_{50} value of 8.57 µM against T47D cells with a selectivity index of 9.73. The action mode of **XO** is predicted through the inhibition of the HER2 receptor, with a binding energy of −45.73 kJ/mol through a stable hydrogen bond with Lys753, as presented by molecular docking and molecular dynamics simulations.

■ ACKNOWLEDGMENTS

Yehezkiel Steven Kurniawan thank for the PhD scholarship provided by the Indonesia Endowment Fund for Education Agency (LPDP), Ministry of Finance, the Republic of Indonesia. The authors greatly appreciate financial support from Universitas Gadjah Mada through Final Project Recognition (RTA) with a grant number of 4161/UN1.P1/Dit-Lit/PT.01.01/2025.

■ CONFLICT OF INTEREST

The authors declare no conflict of interest regarding the publication of this manuscript.

■ AUTHOR CONTRIBUTIONS

Jumina, Harno Dwi Pranowo, and Eti Nurwening Sholikhah did supervision, conceptualization of this work, and provided the resources. Yehezkiel Steven Kurniawan, Ervan Yudha, and Kasta Gurning conducted the experiment. Yehezkiel Steven Kurniawan and Harizal did formal analysis, wrote, and revised the manuscript. All authors agreed to the final version of this manuscript.

■ REFERENCES

[1] Siegel, R.L., Kratzer, T.B., Giaquinto, A.N., Sung, H., and Jemal, A., 2025, Cancer statistics, 2025, *Ca-Cancer J. Clin.*, 75 (1), 10–45.

[2] Bray, F., Laversanne, M., Sung, H., Ferlay, J., Siegel, R.L., Soerjomataram, I., and Jemal, A., 2024, Global cancer statistics 2022: GLOBOCAN estimates of incidence and mortality worldwide for 36 cancers in 185 countries, *Ca-Cancer J. Clin.*, 74 (3), 229–263.

[3] Ferlay, J., Colombet, M., Soerjomataram, I., Parkin, D.M., Piñeros, M., Znaor, A., and Bray, F., 2021, Cancer statistics for the year 2020: An overview, *Int. J. Cancer*, 149 (4), 778–789.

[4] Ministry of Health of the Republic of Indonesia, 2024, *Kasus Malaria di Indonesia*, https://malaria.kemkes.go.id/case#, accessed on May 15, 2025.

[5] Geng, C., Cui, C., Wang, C., Lu, S., Zhang, M., Chen, D., and Jiang, P., 2020, Systematic evaluations of doxorubicin-induced toxicity in rats based on metabolomics, *ACS Omega*, 6 (1), 358–366.

[6] Galfetti, E., Cerutti, A., Ghielmini, M., Zucca, E., and Wannesson, L., 2020, Risk factors for renal toxicity after inpatient cisplatin administration, *BMC Pharmacol. Toxicol.*, 21 (1), 19.

[7] Mielke, H., Algharably, E.A.E., and Gundert-Remy, U., 2025, 5-Fluorouracil toxicity: Revisiting the relevance of pharmacokinetic parameters, *Pharmaceuticals*, 18 (5), 653.

[8] Biguetti, C.C., Junior, J.F.S., Fiedler, M.W., Marrelli, M.T., and Brotto, M., 2021, The toxic effects of chloroquine and hydroxychloroquine on skeletal muscle: A systematic review and meta-analysis, *Sci. Rep.*, 11 (1), 6589.

[9] Fundytus, A., Sengar, M., Lombe, D., Hopman, W., Jalink, M., Gyawali, B., Trapani, D., Roitberg, F., De Vries, E.G.E., Moja, L., Ilbawi, A., Sullivan, R., and Booth, C.M., 2021, Access to cancer medicines deemed essential by oncologists in 82 countries: An international, cross-sectional survey, *Lancet Oncol.*, 22 (10), 1367–1377.

[10] Pandey, S.K., Anand, U., Siddiqui, W.A., and Tripathi, R., 2023, Drug development strategies for malaria: With the hope for new antimalarial drug discovery—An update, *Adv. Med.*, 2023 (1), 5060665.

[11] McVicker, R.U., and O'Boyle, N.M., 2024, Chirality of new drug approvals (2013–2022): Trends and perspectives, *J. Med. Chem.*, 67 (4), 2305–2320.

[12] Kurniawan, Y.S., Priyangga, K.T.A., Jumina, J., Pranowo, H.D., Sholikhah, E.N., Zulkarnain, A.K., Fatimi, H.A., and Julianus, J., 2021, An update on the anticancer activity of xanthone derivatives: A review, *Pharmaceuticals*, 14 (11), 1144.

[13] Kurniawan, Y.S., Amrulloh, H., Yudha, E., Fatmasari, N., Hermawan, F., Fitria, A., Pranowo, H.D., Sholikhah, E.N., and Jumina, J., 2025, Evaluation of xanthone and cinnamoylbenzene as anticancer agents for breast cancer cell lines through in vitro and in silico assays, *J. Multidiscip. Appl. Nat. Sci.*, 5 (1), 87–102.

[14] Konyanee, A., Chaniad, P., Chukaew, A., Payaka, A., Septama, A.W., Phuwajaroanpong, A., Plirat, W., and Punsawad, C., 2024, Antiplasmodial potential of isolated xanthones from *Mesua ferrea* Linn. roots: An *in vitro* and *in silico* molecular docking and pharmacokinetics study, *BMC Complementary Med. Ther.*, 24 (1), 282.

[15] Durães, F., Resende, D.I.S.P., Palmeira, A., Szemerédi, N., Pinto, M.M.M., Spengler, G., and Sousa, E., 2021, Xanthones active against multidrug

resistance and virulence mechanisms of bacteria, *Antibiotics*, 10 (5), 600.

[16] Rząd, K., Ioannidi, R., Marakos, P., Pouli, N., Olszewski, M., Kostakis, I.K., and Gabriel, I., 2023, Xanthone synthetic derivatives with high anticandidal activity and positive mycostatic selectivity index values, *Sci. Rep*., 13 (1), 11893.

[17] Karim, N., Rahman, M.A., Changlek, S., and Tangpong, J., 2020, Short-time administration of xanthone from garcinia mangostana fruit pericarp attenuates the hepatotoxicity and renotoxicity of type II diabetes mice, *J. Am. Coll. Nutr*., 39 (6), 501–510.

[18] Kang, H.H., Zhang, H.B., Zhong, M.J., Ma, L.Y., Liu, D.S., Liu, W.Z., and Ren, H., 2018, Potential antiviral xanthones from a coastal saline soil fungus *Aspergillus iizukae*, *Mar. Drugs*, 16 (11), 449.

[19] Pinto, M.M.M., Palmeira, A., Fernandes, C., Resende, D.I.S.P., Sousa, E., Cidade, H., Tiritan, M.E., Correia-da-Silva, M., and Cravo, S., 2021, From natural products to new synthetic small molecules: A journey through the world of xanthones, *Molecules*, 26 (2), 431.

[20] Plötz, T., von Hanstein, A.S., Krümmel, B., Laporte, A., Mehmeti, I., and Lenzen, S., 2019, Structure-toxicity relationships of saturated and unsaturated free fatty acids for elucidating the lipotoxic effects in human EndoC-βH1 beta-cells, *Biochim. Biophys. Acta, Mol. Basis Dis.*, 1865 (11), 165525.

[21] Fatmayanti, B.R., Jumina, J., Purwono, B., Kurniawan, Y.S., Pranowo, H.D., and Sholikhah, E.N., 2024, Oleate epoxides derived from palm oil as new anticancer agents: Synthesis, cytotoxicity evaluation, and molecular docking studies against FASN protein, *ChemistrySelect*, 9 (17), e202400752.

[22] Sampath Kumar, H.M., Herrmann, L., and Tsogoeva, S.B., 2020, Structural hybridization as a facile approach to new drug candidates, *Bioorg. Med. Chem. Lett*., 30 (23), 127514.

[23] Lundberg, B.B., Risovic, V., Ramaswamy, M., and Wasan, K.M., 2003, A lipophilic paclitaxel derivative incorporated in a lipid emulsion for parenteral administration, *J. Controlled Release*, 86 (1), 93–100.

[24] Huan, M., Zhou, S., Teng, Z., Zhang, B., Liu, X., Wang, J., and Mei, Q., 2009, Conjugation with alpha-linolenic acid improves cancer cell uptake and cytotoxicity of doxorubicin, *Bioorg. Med. Chem. Lett*., 19 (9), 2579–2584.

[25] Barbosa, F., Araújo, J., Gonçalves, V.M.F., Palmeira, A., Cunha, A., Silva, P.M.A., Fernandes, C., Pinto, M., Bousbaa, H., Queirós, O., and Tiritan, M.E., 2024, Evaluation of antitumor activity of xanthones conjugated with amino acids, *Int. J. Mol. Sci*., 25 (4), 2121.

[26] Kurniawan, Y.S., Yudha, E., Jumina, J., Pranowo, H.D., and Sholikhah, E.N., 2025, Synthesis, *in vitro* antimicrobial activity, and *in silico* bioinformatical approach of xanthone-fatty acid esters against *Staphylococcus aureus*, *Escherichia coli*, and *Candida albicans*, *Eur. J. Med. Chem. Rep*., 13, 100245.

[27] Morris, G.M., Huey, R., Lindstrom, W., Sanner, M.F., Belew, R.K., Goodsell, D.S., and Olson, A.J., 2009, AutoDock4 and AutoDockTools4: Automated docking with selective receptor flexibility, *J. Comput. Chem.*, 30 (16), 2785–2791.

[28] Abraham, M.J., Murtola, T., Schulz, R., Páll, S., Smith, J.C., Hess, B., and Lindahl, E., 2015, GROMACS: High performance molecular simulations through multi-level parallelism from laptops to supercomputers, *SoftwareX*, 1-2, 19–25.

[29] BIOVIA, Dassault Systèmes, 2017, *Discovery Studio Visualizer ver. 17.2.0.16349*, Dassault Systèmes, San Diego, US.

[30] Fuhrmann, J., Rurainski, A., Lenhof, H.P., and Neumann, D., 2010, A new Lamarckian genetic algorithm for flexible ligand-receptor docking, *J. Comput. Chem.*, 31 (9), 1911–1918.

[31] Kurniawan, Y.S., Fatmasari, N., Jumina, J., Pranowo, H.D., and Sholikhah, E.N., 2024, Evaluation of the anticancer activity of hydroxyxanthones against human liver carcinoma cell line, *J. Multidiscip. Appl. Nat. Sci*., 4 (1), 1–15.

[32] Huang, J., and MacKerell, A.D.Jr., 2013, CHARMM36 all-atom additive protein force field:

Validation based on comparison to NMR data, *J. Comput. Chem.*, 34 (25), 2135–2145.

[33] Vanommeslaeghe, K., MacKerell, A.D.Jr., 2012, Automation of the CHARMM General Force Field (CGenFF) I: Bond perception and atom typing, *J. Chem. Inf. Model.*, 52 (12), 3144–3154.

[34] Vanommeslaeghe, K., Raman, E.P., and MacKerell, A.D.Jr., 2012, Automation of the CHARMM General Force Field (CGenFF) II: Assignment of bonded parameters and partial atomic charges, *J. Chem. Inf. Model.*, 52 (12), 3155–3168.

[35] Mark, P., and Nilsson, L., 2001, Structure and dynamics of the TIP3P, SPC, and SPC/E water models at 298 K, *J. Phys. Chem. A*, 105 (43), 9954–9960.

[36] Essmann, U., Perera, L., Berkowitz, M.L., Darden, T., Lee, H., and Pedersen, L.G., 1995, A smooth particle mesh Ewald method, *J. Chem. Phys.*, 103 (19), 8577–8593.

[37] Ke, Q., Gong, X., Liao, S., Duan, C., and Li, L., 2022, Effects of thermostats/barostats on physical properties of liquids by molecular dynamics simulations, *J. Mol. Liq.*, 365, 120116.

[38] Kurniawan, Y.S., Fatmasari, N., Pranowo, H.D., Sholikhah, E.N., and Jumina, J., 2024, Investigation on anticancer agent against cervical and colorectal cancer cell lines: One-pot synthesis, *in vitro* and *in silico* assays of xanthone derivatives, *J. Appl. Pharm. Sci.*, 14 (3), 145–153.

[39] Fatmasari, N., Kurniawan, Y.S., Jumina, J., Anwar, C., Priastomo, Y., Pranowo, H.D., Zulkarnain, A.K., and Sholikhah, E.N., 2022, Synthesis and *in vitro* assay of hydroxyxanthones as antioxidant and anticancer agents, *Sci. Rep.*, 12 (1), 1535.

[40] Iresha, M.R., Jumina, J., Pranowo, H.D., Sholikhah, E.N., and Hermawan, F., 2022, Synthesis, cytotoxicity evaluation and molecular docking studies of xanthyl-cinnamate derivatives as potential anticancer agents, *Indones. J. Chem.*, 22 (5), 1407–1417.

[41] Zakiah, M., Syarif, R.A., Mustofa, M., Jumina, J., Fatmasari, N., and Sholikhah, E.N., 2021, *In vitro* antiplasmodial, heme polymerization, and cytotoxicity of hydroxyxanthone derivatives, *J. Trop. Med.*, 2021 (1), 8866681.

[42] Liu, J., Zhang, J., Wang, H., Liu, Z., Zhang, C., Jiang, Z., and Chen, H., 2017, Synthesis of xanthone derivatives and studies on the inhibition against cancer cells growth and synergistic combinations of them, *Eur. J. Med. Chem.*, 133, 50–61.

[43] Yuanita, E., Pranowo, H.D., Mustofa, M., Swasono, R.T., Syahri, J., and Jumina, J., 2019, Synthesis, characterization and molecular docking of chloro-substituted hydroxyxanthone derivatives, *Chem. J. Mold.*, 14 (1), 68–76.

[44] Tanamatayarat, P., Limtrakul, P., Chunsakaow, S., and Duangrat, C., 2003, Screening of some rubiaceous plants for cytotoxic activity against cervic carcinoma (KB-3-1) cell line, *Thai J. Pharm. Sci.*, 27 (3), 167–172.

[45] Widiandani, T., Tandian, T., Zufar, B.D., Suryadi, A., Purwanto, B.T., Hardjono, S., and Siswandono, S., 2023, *In vitro* study of pinostrobin propionate and pinostrobin butyrate: Cytotoxic activity against breast cancer cell T47D and its selectivity index, *J. Public Health Afr.*, 14 (S1), 2516.

[46] Batista, R., De Jesus Silva Júnior, A., and De Oliveira, A.B., 2009, Plant-derived antimalarial agents: new leads and efficient phytomedicines. Part II. Non-alkaloidal natural products, *Molecules*, 14 (8), 3037–3072.

[47] Xia, X., Gong, C., Zhang, Y., and Xiong, H., 2023, The history and development of HER2 inhibitors, *Pharmaceuticals*, 16 (10), 1450.

[48] Horimoto, Y., Ishizuka, Y., Ueki, Y., Higuchi, T., Arakawa, A., and Saito, M., 2022, Comparison of tumors with HER2 overexpression versus HER2 amplification in HER2-positive breast cancer patients, *BMC Cancer*, 22 (1), 242.

[49] Aman, N.A., Doukoure, B., Koffi, K.D., Koui, B.S., Traore, Z.C., Kouyate, M., and Effi, A.B., 2019, HER2 overexpression and correlation with other significant clinicopathologic parameters in Ivorian breast cancer women, *BMC Clin. Pathol.*, 19 (1), 1.

[50] Chen, F.M., Huang, L.J., Ou-Yang, F., Kan, J.Y., Kao, L.C., and Hou, M.F., 2020, Activation of

mitochondrial unfolded protein response is associated with Her2-overexpression breast cancer, *Breast Cancer Res. Treat*., 183, 61–70.

[51] Ibragimova, K.I.E., Geurts, S.M.E., Meegdes, M., Erdkamp, F., Heijns, J.B., Tol, J., Vriens, B.E.P., Dercksen, M.W., Aaldering, K.N.A., Pepels, M.J.A.E., van de Winkel, L., Peters, N.A.J.B., Teeuwen-Dedroog, N.J.A., Vriens, I.J.H., and Tjan-Heijnen, V.C.G., 2023, Outcomes for the first four lines of therapy in patients with HER2-positive advanced breast cancer: Results from the SONABRE registry, *Breast Cancer Res. Treat.*, 198 (2), 239–251.

[52] Sharaf, B., Tamimi, F., Al-Abdallat, H., Khater, S., Salama, O., Zayed, A., El Khatib, O., Qaddoumi, A., Horani, M., AL-Masri, Y., Asha, W., Altalla', B., Bani Hani, H., and Abdel-Razeq, H., 2025, Dual anti-HER2 therapy vs trastuzumab alone with neoadjuvant anthracycline and taxane in HER2-positive early-stage breast cancer: Real-world insights, *Biol.: Targets Ther.*, 19, 59–71.

[53] Aertgeerts, K., Skene, R., Yano, J., Sang, B.C., Zou, H., Snell, G., Jennings, A., Iwamoto, K., Habuka, N., Hirokawa, A., Ishikawa, T., Tanaka, T., Miki, H., Ohta, Y., and Sogabe, S., 2011, Structural analysis of the mechanism of inhibition and allosteric activation of the kinase domain of HER2 protein, *J. Biol. Chem.*, 286 (21), 18756–18765.

[54] Fitria, A., Kurniawan, Y.S., Ananto, A.D., Jumina, J., Sholikhah, E.C., and Pranowo, H.D., 2025, Allyl-modified of calix[4]resorcinarene derivatives for HER2 inhibition agents: An *in silico* study, *J. Multidiscip. Appl. Nat. Sci.*, 5 (2), 352–369.

[55] Sinha, S., Tam, B., and Wang, S.M., 2022, Applications of molecular dynamics simulation in protein study, *Membranes*, 12 (9), 844.

[56] Aier, I., Varadwaj, P.K., and Raj, U., 2016, Structural insights into conformational stability of both wild-type and mutant EZH2 receptor, *Sci. Rep.*, 6 (1), 34984.

[57] Fatriansyah, J.F., Boanerges, A.G., Kurnianto, S.R., Pradana, A.F., Fadilah, F., and Surip, S.N., 2022, Molecular dynamics simulation of ligands from *Anredera cordifolia* (binahong) to the main protease (M^{pro}) of SARS-CoV-2, *J. Trop. Med.*, 2022 (1), 1178228.

[58] Kurniawan, Y.S., Yudha, E., Nugraha, G., Fatmasari, N., Pranowo, H.D., Jumina, J., and Sholikhah, E.N., 2024, Molecular docking and molecular dynamic investigations of xanthone-chalcone derivatives against epidermal growth factor receptor for preliminary discovery of novel anticancer agent, *Indones. J. Chem.*, 24 (1), 250–266.

[59] Yogaswara, R., Pranowo, H.D., Prasetyo, N., and Pulung, M.L., 2025, Investigation of new 4-benzyloxy-2-trichloromethylquinazoline derivatives as *Plasmodium falciparum* dihydrofolate reductase-thymidylate synthase inhibitors: QSAR, ADME, drug-likeness, toxicity, molecular docking and molecular dynamics simulation, *J. Multidiscip. Appl. Nat. Sci.*, 5 (2), 456–486.

[60] Pulung, M.L., Swasono, R.T., Sholikhah, E.N., Yogaswara, R., Primahana, G., and Raharjo, T.J., 2025, Antiplasmodial and metabolite profiling of *Hyrtios* sp. sponge extract from Southeast Sulawesi marine using LC-HRMS, molecular docking, pharmacokinetic, drug-likeness, toxicity, and molecular dynamics simulation, *J. Multidiscip. Appl. Nat. Sci.*, 5 (2), 487–508.